



Adipocyte-Specific Deletion of Lamin A/C Largely Models Human Familial Partial Lipodystrophy Type 2

Callie A.S. Corsa,¹ Carolyn M. Walsh,¹ Devika P. Bagchi,¹ Maria C. Foss Freitas,² Ziru Li,¹ Julie Hardij,¹ Katrina Granger,¹ Hiroyuki Mori,¹ Rebecca L. Schill,¹ Kenneth T. Lewis,¹ Jessica N. Maung,¹ Ruth D. Azaria,¹ Amy E. Rothberg,² Elif A. Oral,² and Ormond A. MacDougald^{1,2}

Diabetes 2021;70:1970–1984 | <https://doi.org/10.2337/db20-1001>

Mechanisms by which autosomal recessive mutations in *Lmna* cause familial partial lipodystrophy type 2 (FPLD2) are poorly understood. To investigate the function of lamin A/C in adipose tissue, we created mice with an adipocyte-specific loss of *Lmna* (*Lmna*^{ADKO}). Although *Lmna*^{ADKO} mice develop and maintain adipose tissues in early post-natal life, they show a striking and progressive loss of white and brown adipose tissues as they approach sexual maturity. *Lmna*^{ADKO} mice exhibit surprisingly mild metabolic dysfunction on a chow diet, but on a high-fat diet they share many characteristics of FPLD2 including hyperglycemia, hepatic steatosis, hyperinsulinemia, and almost undetectable circulating adiponectin and leptin. Whereas *Lmna*^{ADKO} mice have reduced regulated and constitutive bone marrow adipose tissue with a concomitant increase in cortical bone, FPLD2 patients have reduced bone mass and bone mineral density compared with controls. In cell culture models of *Lmna* deficiency, mesenchymal precursors undergo adipogenesis without impairment, whereas fully differentiated adipocytes have increased lipolytic responses to adrenergic stimuli. *Lmna*^{ADKO} mice faithfully reproduce many characteristics of FPLD2 and thus provide a unique animal model to investigate mechanisms underlying *Lmna*-dependent loss of adipose tissues.

Lipodystrophy syndromes are rare diseases characterized by generalized or partial loss of adipose tissues, accompanied by metabolic alterations secondary to insulin resistance including lipodystrophy-related diabetes, hyperlipidemia, and nonalcoholic fatty liver disease (1–9). The most

common form of monogenic lipodystrophy is familial partial lipodystrophy type 2 (FPLD2), which is caused by autosomal dominant mutations in the *Lmna* gene encoding nuclear lamins A and C. FPLD2 patients generally have heterozygous or compound heterozygous variants affecting exons 8 and 11 of *Lmna*. Variants in exon 8, including position R482, are associated with 80% of FPLD2 cases and produce a severe lipodystrophic phenotype (10–14). Strong disease phenotypes have also been described for autosomal-dominant non-R482 single missense mutations and for homozygous pathogenic variants; less severe metabolic disease phenotypes have been associated with mutations in other *Lmna* exons (15,16). Although *Lmna* mutations alter functional aspects of nuclear structure, chromosome organization, and transcription factor activity, mechanisms by which lamin A/C mutations cause lipoatrophy remain incompletely understood.

Overexpression of wild-type lamin A or R482 mutants in 3T3-L1 cells is sufficient to inhibit preadipocyte differentiation (2). Transgenic mice that overexpress the most common FPLD2 *Lmna* mutation (R482Q) in adipose tissue have characteristics similar to the human phenotype, including loss of adipose tissue, glucose intolerance, insulin resistance, and fatty liver; however, these phenotypes develop slowly and are relatively mild, even on a high-fat diet (HFD) (1). On the other hand, precursor cells isolated from lamin^{-/-} mice also have diminished capacity for adipogenesis, as do induced pluripotent stem cells lines derived from patients with FPLD2 (5,17), and mice with global deletion of *Lmna* lack white adipose tissue (WAT).

¹Department of Molecular & Integrative Physiology, University of Michigan, Ann Arbor, MI

²Division of Metabolism, Endocrinology and Diabetes, Department of Internal Medicine, University of Michigan, Ann Arbor, MI

Corresponding author: Ormond A. MacDougald, maccdouga@umich.edu

Received 2 October 2020 and accepted 25 May 2021

This article contains supplementary material online at <https://doi.org/10.2337/figshare.14691045>.

C.A.S.C. and C.M.W. contributed equally to this work.

© 2021 by the American Diabetes Association. Readers may use this article as long as the work is properly cited, the use is educational and not for profit, and the work is not altered. More information is available at <https://www.diabetesjournals.org/content/license>.

Unfortunately, whole-body lamin^{-/-} mice are a challenging experimental model to interpret, as they are runted, have severe musculoskeletal defects, and die by 6–8 weeks of age (3,4). Thus, more sophisticated animal models are required to evaluate mechanisms of lipodystrophy, since both gain- and loss-of-function approaches for lamin A/C mutations cause impaired adipogenesis of cultured cells and depletion of adipose tissue in mice.

Herein we report that mice with selective deletion of floxed *Lmna* in adipocytes (*Lmna*^{ADKO}) develop functional WAT and brown adipose tissue (BAT) depots postnatally but lose the vast majority of adipocytes coincident with sexual maturity. While both male and female *Lmna*^{ADKO} mice develop lipodystrophy and metabolic dysfunction, effects are more pronounced on an HFD and in females, mirroring the sex differences observed in FPLD2 patients. Although the phenotype of *Lmna*^{ADKO} mice is highly correlated with clinical signs of FPLD2, some characteristics are more reminiscent of acquired generalized lipodystrophy. In addition, cortical bone mass is increased in *Lmna*^{ADKO} mice, whereas we observed reduced bone mass in FPLD2 patients. Adipogenesis of primary *Lmna*-deficient precursors is not impaired; however, adrenergic-stimulated lipolysis of resulting adipocytes is slightly increased. Together, these data in mice demonstrate that when knocked out during adipogenesis, lamin A/C is not required for development of adipocytes early in life but is necessary for the maintenance of adipose tissue and metabolic homeostasis in adulthood.

RESEARCH DESIGN AND METHODS

Animals

Homozygous *Lmna*^{FL} mice had loxP sites flanking exons 10 and 11 of the *Lmna* allele (18). Adipoq-Cre mice were from the Jackson Laboratory (catalog no. 028020; Ellsworth, ME) (19). Animals described as *Lmna*^{CTRL} were a mix of *Lmna*^{FL};Adipoq-Cre⁻ and *Lmna*^{FL/+};Adipoq-Cre⁺ mice. No phenotype was observed in *Lmna*^{FL/+};Adipoq-Cre⁺ mice. Body composition was measured with nuclear magnetic resonance spectroscopy, and energy balance was estimated with the Comprehensive Lab Animal Monitoring System (CLAMS) in the University of Michigan Mouse Metabolic Phenotyping Core. Animals were group housed under standard conditions with a 12-h light:dark cycle and free access to chow and water. For HFD challenge, mice were fed a diet containing 60% calories from fat for 5 weeks (catalog no. 12492; Research Diets, New Brunswick, NJ). All animal studies were performed in compliance with policies of the University of Michigan Institutional Animal Care and Use Committee (protocol no. PRO00009687).

Human Participants and Study Design

For this retrospective case-control study, we included patients with a heterozygous mutation in the *LMNA* hotspot codon Arg482 (R482 group) in exon 8 and individuals without lipodystrophy as a control group matched for

age, sex, and BMI. Data regarding demographic information, metabolic abnormality, and body composition were collected from clinical records obtained from the University of Michigan, Ann Arbor, Michigan, after patients gave informed consent. The University of Michigan Institutional Review Board approved the study. Control patients were enrolled in a 2-year intensive behavioral weight management program, which has been described elsewhere (20). FPLD2 patients are part of a long-term observational, international, multicenter, prospective study collecting data on the natural history of different lipodystrophy syndromes (LD-Lync; clinical trial reg. no. NCT03087253, clinicaltrials.gov). DEXA data, available from 24 R482 patients and 18 control individuals matched by age, sex, and BMI, were evaluated for body composition, as well as bone variables. Statistical comparisons between matched cohorts were made using the Wilcoxon rank sum test, and data are presented as mean ± SD. Values were considered to be statistically significant when $P < 0.05$. DEXA parameters were also evaluated from 24 patients from the R482 group and 18 from the control group.

Cell Culture

Primary mesenchymal stem cells from *Lmna*^{FL} mice were isolated, cultured, and differentiated as previously described (21,22). For Cre-mediated deletion of *Lmna*, precursors were treated with 1×10^{10} adenoviral particles/mL expressing either GFP (Adeno-GFP) or Cre recombinase (Adeno-Cre) for 48 h in serum-free media. Adenoviral treatment was begun 1–2 days after plating cells and completed prior to induction of adipogenesis. Oil Red O staining to visualize neutral lipid accumulation was performed as described previously (23).

Immunofluorescence

For Mac2/Cav1 immunofluorescent staining, freshly isolated posterior subcutaneous WAT (psWAT) and gonadal WAT (gWAT) were minced into small pieces (~5 mg) and fixed overnight in 1% paraformaldehyde at 4°C. The tissues were then washed three times with PBS, incubated in blocking solution (PBS, 5% BSA, and 0.3% Triton X-100) for 1 h at room temperature, and incubated in primary antibodies (diluted 1:300 in blocking solution) overnight at 4°C. The tissues were washed three times with blocking solution and then incubated with Alexa Fluor-conjugated secondary antibodies (diluted 1:300 in blocking solution) for 1 h at room temperature, protected from light. The tissues were washed two times with PBS, stained with 150 nmol/L Hoechst in PBS for 10 min, washed two times with PBS, and immediately imaged using confocal microscopy (Nikon A1). Antibody information is listed in Supplementary Table 1.

Analyses of Bone and Bone Marrow Adipose Tissue

Bones from *Lmna*^{FL} and *Lmna*^{ADKO} mice were fixed in 10% neutral buffered formalin for 24 h and then washed

three times with water and placed in Sorenson phosphate buffer (0.1 mol/L; pH 7.4) as previously described (24,25). Tibiae were placed in a specimen holder 19 mm in diameter and scanned over their entire length using a microcomputed tomography (μ CT) system (μ CT100 Scanco Medical). Scan settings were as follows: voxel size 12 μ m, 70 kVp, 114 μ A, 0.5-mm AL filter, and integration time 500 ms. Density measurements were calibrated to the manufacturer's hydroxyapatite phantom. Analyses were performed using the manufacturer's evaluation software and a threshold of 180 for trabecular bone and 280 for cortical bone. Osmium tetroxide staining and quantification of bone marrow adipose tissue (BMAT) by μ CT were performed as described previously (24,25).

Statistics for Animal Studies

Data are presented as mean \pm SD unless otherwise noted and were analyzed by the two-tailed Student *t* test or ANOVA, unless otherwise indicated. Data collected using indirect calorimetry are presented as mean \pm SEM and were analyzed by ANCOVA using the CalR platform with lean body mass as a covariate. Differences were considered significant at $P < 0.05$ or as indicated in figure legends.

Data and Resource Availability

All reagents and data from this article are available from the corresponding author upon request.

RESULTS

Lmna Deletion in Adipocytes Causes Loss of Adipose Tissue

To investigate the importance of lamin A/C in adipose tissue, we developed a model to delete *Lmna* in adipocytes (*Lmna*^{ADKO}) by breeding Adipoq-Cre mice with mice containing floxed *Lmna* alleles (*Lmna*^{FL}) (Supplementary Fig. 1A–E). We confirmed through genotyping and immunoblot analyses that lamin A/C is lost specifically from adipocytes of sWAT in mice at 4 weeks of age (Supplementary Fig. 1B and E). To determine whether recombination of exons 10 and 11 results in a truncated lamin protein, we infected cultured mesenchymal precursors from *Lmna*^{FL} mice with an adenovirus expressing Cre recombinase (Adeno-Cre) or GFP (Adeno-GFP) prior to adipogenesis. Immunoblot analyses with an N-terminal antibody to lamin A/C revealed a robust band in lysates from Adeno-GFP-infected cells but not from Adeno-Cre-infected cells, even at high exposure (Supplementary Fig. 1C). We then asked whether the mRNA expression of truncated *Lmna* might be altered in cells treated with Adeno-Cre and observed that mutant *Lmna* was expressed comparably to wild-type *Lmna* mRNA (Supplementary Fig. 1D). These data suggest that the truncated protein is rapidly degraded. At 12–14 weeks of age, visual inspection revealed that male *Lmna*^{ADKO} mice have a striking loss of WAT, including

psWAT, anterior sWAT, and gWAT (epididymal or ovarian) depots (Fig. 1A and Supplementary Fig. 1F). In addition, interscapular BAT was smaller and whiter in appearance. The livers of *Lmna*^{ADKO} were enlarged and paler in color (Fig. 1A and Supplementary Fig. 1F). Adipocyte-specific deletion of *Lmna* did not substantially affect total body weight of either sex (Fig. 1B) but, in females, led to a change in body composition, with decreased fat mass and elevated lean mass (Fig. 1C). Consistent with visual inspection, loss of lamin A/C in adipocytes led to a profound reduction in weight of psWAT, gWAT, and mesenteric, pericardial, renal, and retroperitoneal WAT in both sexes (Fig. 1D and E and Supplementary Fig. 1F; data not shown). Although male mice had reduced BAT and increased liver weight, significant differences in weights of these tissues were not observed in female mice (Fig. 1F and G). Heart, pancreas, and spleen did not have grossly altered appearances, and although heart weights were increased in both sexes, weights of pancreas and spleen were unaltered (Supplementary Fig. 1G–I). Histological analyses of WAT remnants from *Lmna*^{ADKO} mice revealed an almost complete loss of adipocytes, along with an increase of fibrotic stroma (Fig. 1H). In both sexes, the BAT of *Lmna*^{ADKO} mice acquired a whitened phenotype with the appearance of large, unilocular adipocytes (Fig. 1H). Liver showed mild hepatosteatosis, and dermal adipocytes were completely absent (Fig. 1H). We did not detect a phenotype in heterozygous *Lmna*^{FL/+};Adipoq-Cre mice (data not shown), consistent with previous findings that heterozygous global null *Lmna*^{+/-} mice do not have lipodystrophy or metabolic dysfunction (26). Taken together, these data demonstrate that loss of lamin A/C in adipocytes causes a lipodystrophic phenotype in mice.

On a Chow Diet, *Lmna*^{ADKO} Mice Exhibit Only Mild Metabolic Dysregulation

FPLD2 patients have significant metabolic complications including clinical diabetes and nonalcoholic fatty liver disease (7–9); thus, we next investigated effects of adipocyte-specific loss of lamin A/C on whole-body metabolism in mice. Surprisingly, glucose tolerance of *Lmna*^{ADKO} mice was not different between genotypes, although area under the curve suggested glucose intolerance in female mice (Fig. 2A and B and Supplementary Fig. 2A). Whereas fasting blood glucose concentrations were elevated in *Lmna*^{ADKO} mice of both sexes (Fig. 2C), glucose and insulin concentrations were only higher in random-fed female mice (Fig. 2C and D). Adiponectin was undetectable in the serum of *Lmna*^{ADKO} mice (Fig. 2E), but there was only a trend toward reduced leptin concentrations (Supplementary Fig. 2B). Adipocyte-specific deletion of *Lmna* led to increased serum triacylglycerols in female mice and decreased glycerol in both sexes (Fig. 2F and G). We next measured circulating glycerol concentrations following administration of isoproterenol. *Lmna*^{ADKO} mice of both sexes had lower concentrations of serum glycerol than *Lmna*^{CTRL} mice

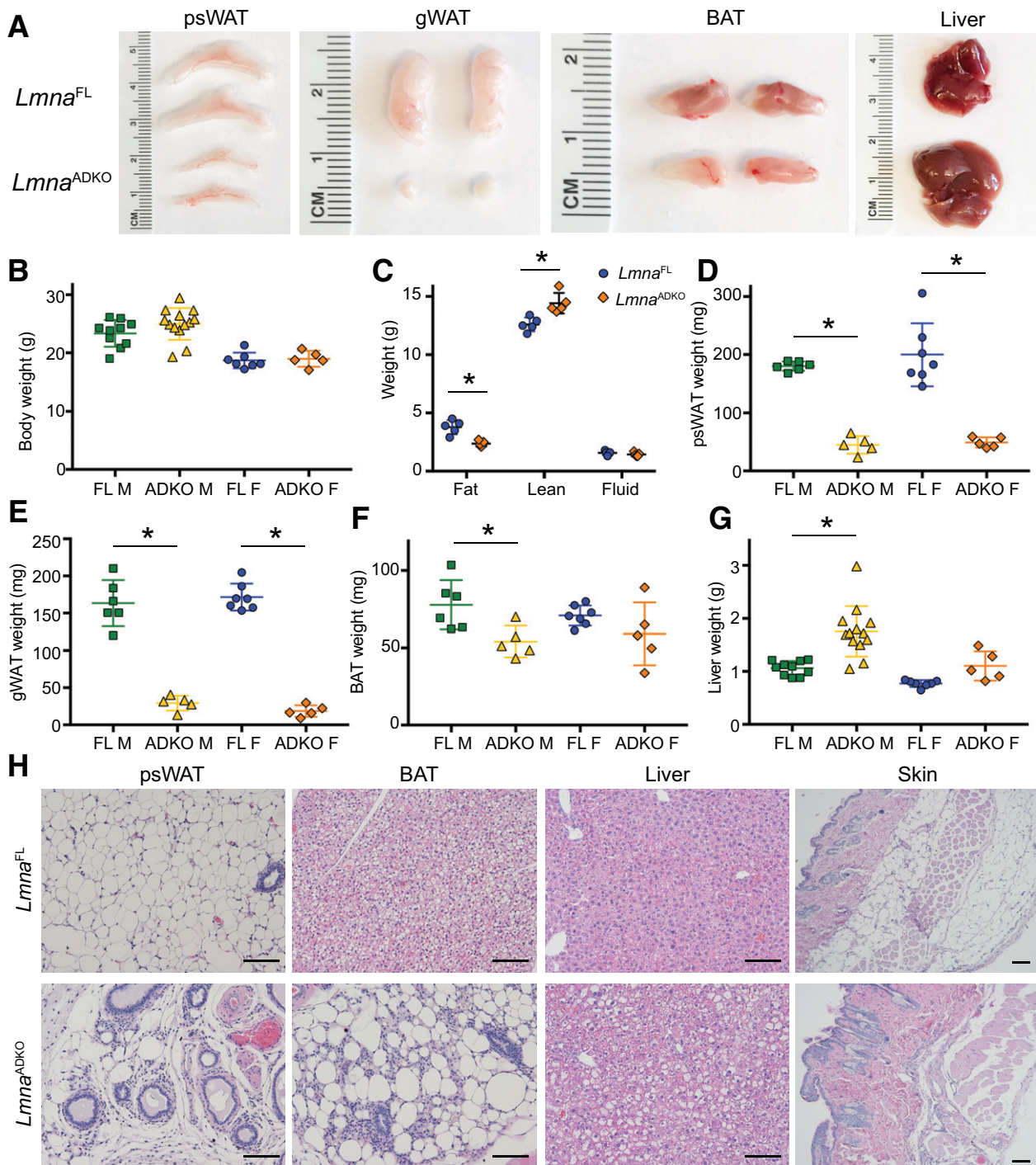


Figure 1—Adipocyte-specific deletion of lamin A/C leads to loss of adipose tissues in mice. *A*: Representative images of psWAT, gWAT, BAT, and liver from *Lmna*^{FL} and *Lmna*^{ADKO} male mice 12–14 weeks of age on a normal chow diet. *B*: Body weight of *Lmna*^{FL} and *Lmna*^{ADKO} mice 12–14 weeks of age. *C*: Body composition measured by nuclear magnetic resonance spectroscopy in female *Lmna*^{FL} and *Lmna*^{ADKO} mice 12 weeks of age. *D–G*: Tissue weight of *Lmna*^{FL} and *Lmna*^{ADKO} male and female mice 12–14 weeks of age for psWAT (*D*), gWAT (*E*), BAT (*F*), and liver (*G*). *H*: Representative histologic images of the indicated tissues and organs stained with hematoxylin-eosin from *Lmna*^{FL} and *Lmna*^{ADKO} female mice 12–14 weeks of age. Scale bars 100 μ mol/L. **P* < 0.05. F, female; M, male.

at baseline and a blunted increase in response to isoproterenol, indicating an impaired capacity for lipolysis (Supplementary Fig. 2*D* and *G*). However, normalization of glycerol concentrations to total WAT weight suggests the

adipocytes present may have been highly lipolytic (Supplementary Fig. 2*E* and *H*). To evaluate whether mice develop more severe metabolic complications with age, we performed glucose and insulin tolerance tests in female

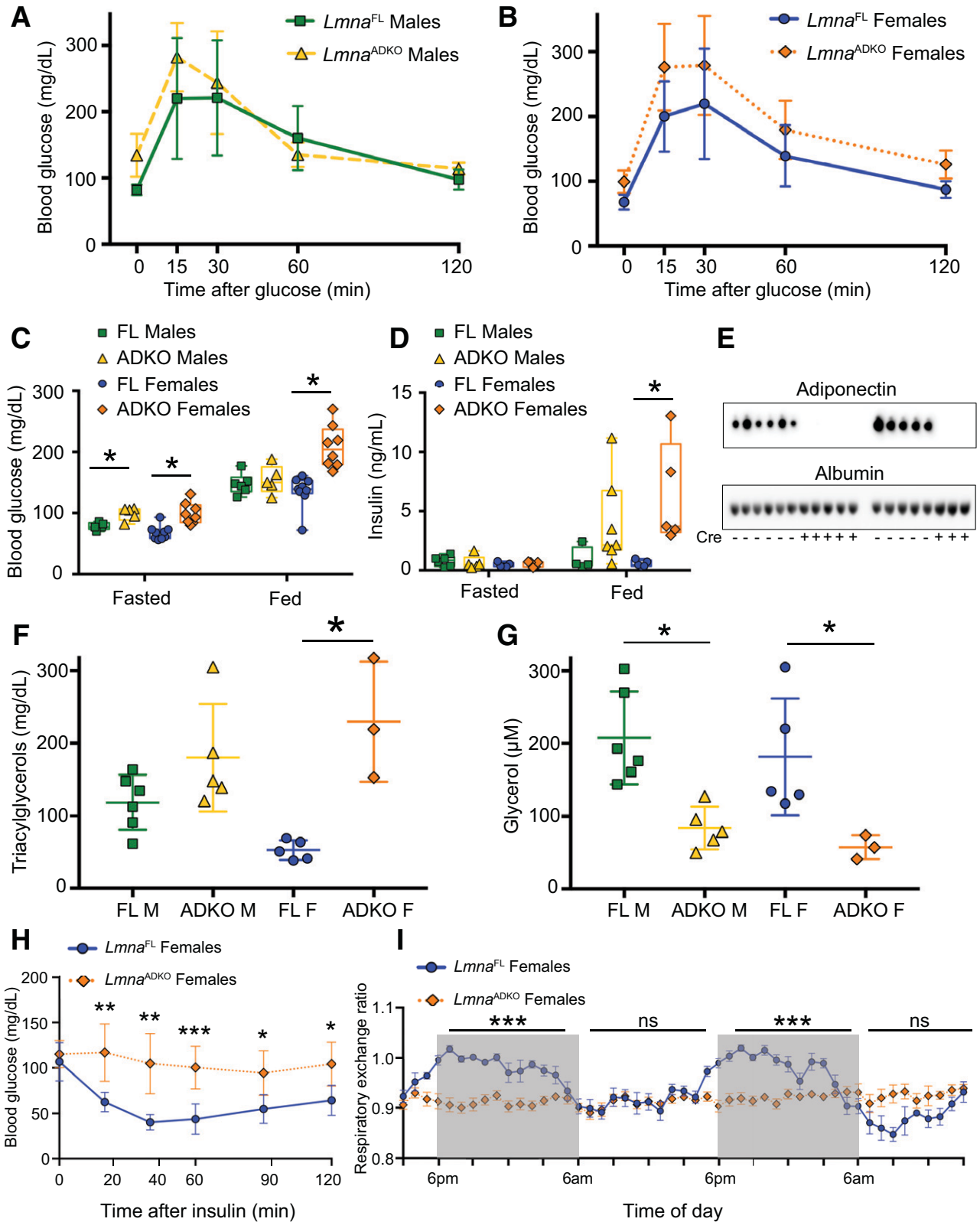


Figure 2—*Lmna*^{ADKO} mice display mild metabolic dysregulation on a normal chow diet. *A* and *B*: Glucose tolerance tests for male (*A*) and female (*B*) *Lmna*^{FL} and *Lmna*^{ADKO} mice 14 weeks of age. *C* and *D*: Circulating glucose (*C*) and insulin concentrations (*D*) in *Lmna*^{FL} and *Lmna*^{ADKO} mice 12–14 weeks of age with ad libitum feeding or following a 16-h fast. *E*–*G*: Circulating adiponectin (*E*) and concentrations of triacylglycerol (*F*) and glycerol (*G*) in serum of *Lmna*^{FL} and *Lmna*^{ADKO} mice 12–14 weeks of age. *H*: Insulin tolerance test for female *Lmna*^{FL} and *Lmna*^{ADKO} mice ~6 months of age. *I*: Respiratory exchange ratio (VCO₂/V_{O₂}) for female *Lmna*^{FL} and *Lmna*^{ADKO} mice ~6 months of age; statistical analysis was by ANCOVA with lean body mass as a covariate; data presented as mean ± SEM. **P* < 0.05, ***P* < 0.01, ****P* < 0.001. F, female; M, male; ns, not significant.

Lmna^{FL} and *Lmna*^{ADKO} mice at ~6 months of age and found that while *Lmna*^{ADKO} mice were highly insulin resistant, their glucose tolerance did not differ from that of controls (Fig. 2H and Supplementary Fig. 2I). Taken together, these results indicate that *Lmna*^{ADKO} mice have a mild dysregulation of glucose and lipid metabolism that is more pronounced in females than in males.

Dramatic energy balance alterations have been observed in other mouse models of lipodystrophy, including a “flattened” respiratory exchange ratio (RER), hyperphagia, metabolic inflexibility in switching between oxidation of carbohydrates and fat, and changes in energy expenditure (27–30). We therefore used CLAMS analyses to investigate energy balance in female *Lmna*^{FL} and *Lmna*^{ADKO} mice ~6 months of age. RER in the *Lmna*^{ADKO} animals remained constant at ~0.9 throughout the light and dark cycles, in stark contrast to the cyclical RER observed in control animals (Fig. 2J). In keeping with these observations, *Lmna*^{ADKO} mice had significantly lower rates of oxygen consumption than *Lmna*^{FL} mice during the light cycle and were metabolically inflexible, with an almost constant oxidation of fat and glucose throughout the light and dark cycles (Supplementary Fig. 2J–L). Food consumption, water consumption, and physical activity were not altered in *Lmna*^{ADKO} animals (Supplementary Fig. 2M; data not shown).

Adipocyte-Specific Deletion of *Lmna* Causes Loss of BMAT and Increased Cortical Bone

Whether lipodystrophy extends to BMAT depends on the underlying cause; BMAT is lost in patients with mutations in AGPAT1 or seipin but is maintained in patients with mutations in caveolin or cavin1 (31). In FPLD2 patients, MRI scans suggest that BMAT is also comparable to that of healthy controls (32). To determine whether adipocyte-specific loss of lamin A/C influences BMAT, we histologically evaluated the marrow niche following bone decalcification. We observed a striking loss of regulated bone marrow adipocytes in the distal femur and proximal tibia (Fig. 3A and B and Supplementary Fig. 3A) and a surprising decrease in constitutive BMAT of distal tibia and caudal vertebra (Fig. 3C and D), which generally are resistant to depletion (25). Indeed, quantification with osmium staining revealed a significant reduction in distal tibial BMAT of both male and female animals (Supplementary Fig. 3B). Clinical correlations often show a reciprocal relationship between BMAT and bone mass (33). μ CT analysis of distal tibia revealed increased cortical area and cortical thickness in female *Lmna*^{ADKO} mice (Fig. 3E–G), although no differences were observed in trabecular bone variables of proximal tibia (Supplementary Fig. 3). Together, these data indicate that in mice, lamin A/C is required for development or maintenance of regulated and constitutive BMAT and that loss of BMAT is associated with an increase in cortical bone, although the systematic effects could not be excluded.

FPLD2 Patients With R482 Mutations Have Reduced Fat Mass, Bone Mass, and Bone Mineral Density

To determine whether FPLD2 patients also have increased bone, we retrospectively evaluated 24 FPLD2 patients with the R482 mutation and 18 control patients without lipodystrophy, matched for age, sex, and BMI. Average age of the control and R482 groups was ~50 years, with ~70% women in both cohorts (Supplementary Fig. 4A). Unlike *Lmna*^{ADKO} mice on a normal chow diet, the human population had substantial metabolic dysfunction; 76.2% of R482 patients had type 2 diabetes, and 71.4% were diagnosed with fatty liver, whereas 23.8% and 19.0% of controls were diagnosed with type 2 diabetes and fatty liver, respectively. All patients with R482 mutations had dyslipidemia, compared with 40.5% of patients in the control group. Serum triglycerides were significantly higher in R482 patients (Supplementary Fig. 4B), and HDL cholesterol levels were lower in this group (Supplementary Fig. 4A). Although patients with R482 pathogenic variants were not different in weight, height, BMI, trunk mass index, or fat-free mass index (Fig. 4A and Supplementary Fig. 4A), the fat mass index and trunk fat mass index were significantly lower in the R482 group (Supplementary Fig. 4A and C). As expected, fat mass of FPLD2 patients was significantly lower in arms, legs, trunk, and total body (Fig. 4A). Interestingly, bone mineral density was lower in R482 patients (Fig. 4B), and bone mass of the arms, legs, trunk, and total body were also significantly lower in patients with R482 mutations (Fig. 4C–F). These data indicate a discordance between effects on bone of lamin A/C deficiency in *Lmna*^{ADKO} mice and global mutations of LMNA on R482 in humans. Thus, reduced bone mass in humans may be secondary to metabolic dysfunction or perhaps R482 mutation in osteoblasts or other nonadipocyte populations.

HFD Worsens Lipodystrophy of *Lmna*^{ADKO} Mice

Based on mouse models with chronic (34–36) or acute (37,38) deficiency of adipose tissue, *Lmna*^{ADKO} mice on a chow diet have a surprisingly mild metabolic phenotype. Thus, we next tested whether an HFD would exacerbate the metabolic phenotype, given that inability to store excess energy is a well-established stimulus for disrupting metabolic homeostasis (39). Due to the sex-specific differences in phenotype observed earlier, we conducted these experiments in female animals. Although female *Lmna*^{ADKO} mice only tended toward less weight gain during 5 weeks of HFD feeding (Fig. 5A), these mice lacked detectable WAT depots, including psWAT, gWAT, and mesenteric and pericardial WAT (Supplementary Fig. 5A; data not shown). Livers of *Lmna*^{ADKO} mice following HFD feeding were significantly heavier (Fig. 5B and Supplementary Fig. 5A) and, by histological analyses, showed lipid droplet voids indicative of hepatic steatosis (Fig. 5C). BAT of *Lmna*^{ADKO} mice following HFD feeding also showed evidence of fibrosis and had a whitened appearance, presumably due to the

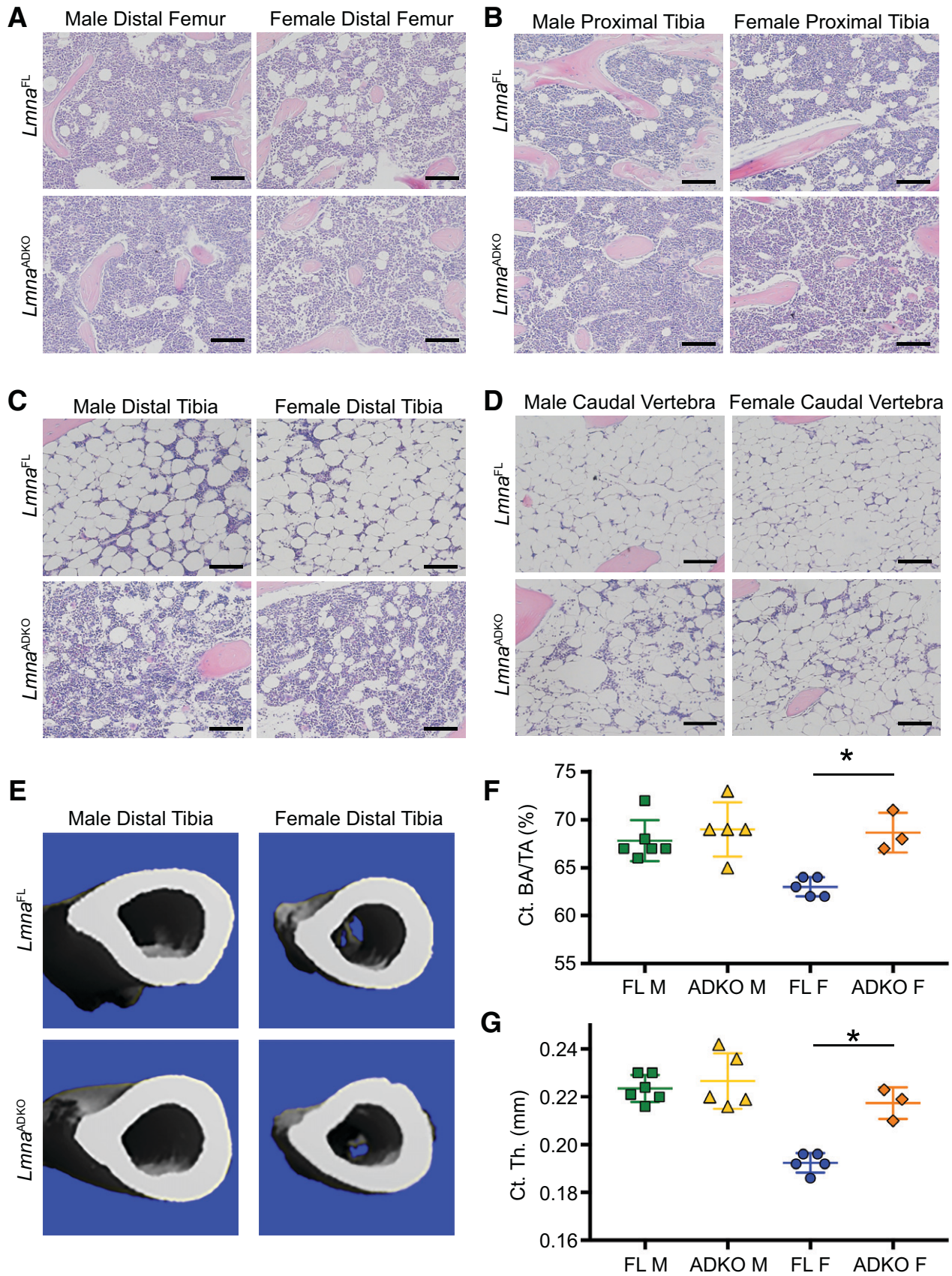


Figure 3—Adipocyte-specific deletion of *Lmna* causes loss of regulated and constitutive BMAT and increases cortical bone. *A–D*: Representative histologic sections stained with hematoxylin-eosin for distal femur (*A*), proximal tibia (*B*), distal tibia (*C*), and caudal vertebra (*D*) from *Lmna*^{FL} and *Lmna*^{ADKO} mice 12–14 weeks of age. Scale bar 100 μ m. *E*: Representative μ CT scans of the distal tibiae from *Lmna*^{FL} and *Lmna*^{ADKO} mice 12–14 weeks of age. *F* and *G*: Cortical bone area per total bone area (*F*) and cortical thickness (*G*) in *Lmna*^{FL} and *Lmna*^{ADKO} mice 12–14 weeks of age. **P* < 0.05. F, female; M, male.

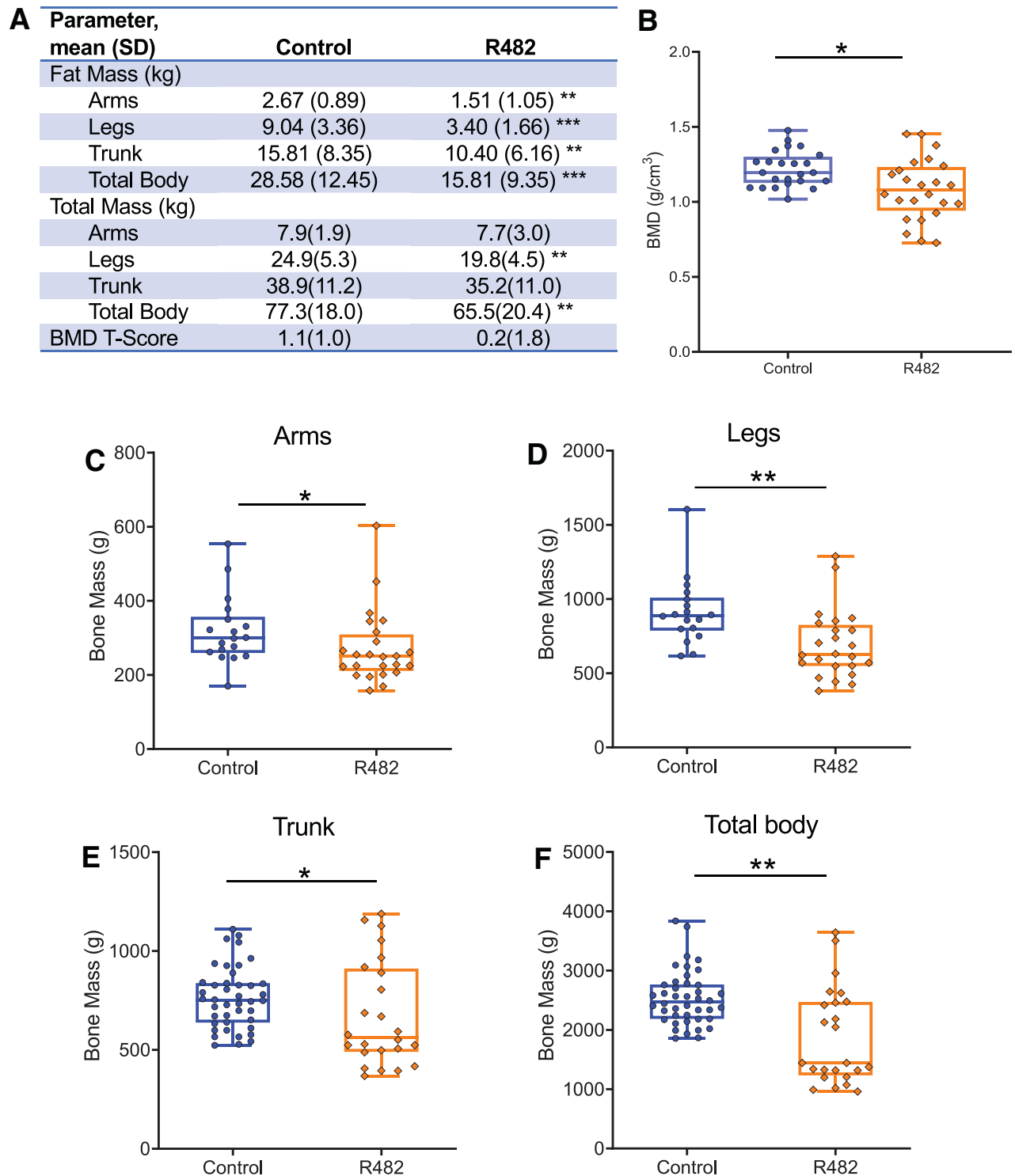


Figure 4—Fat mass, bone mass, and bone mineral density are reduced in patients with R482 mutations in the *LMNA* gene. *A*: Fat mass and total mass of arms, legs, trunk, and total body in control and R482 patients. *B*: Bone mineral density in control (*n* = 18) and R482 patients (*n* = 24). *C–F*: Bone mass in control (*n* = 18) and R482 patients (*n* = 24) in the arms (*C*), legs (*D*), trunk (*E*), and total body (*F*). **P* < 0.05, ***P* < 0.01, ****P* < 0.001. BMD, bone mineral density.

presence of large unilocular lipid droplets (Fig. 5C). It was challenging to identify even a few adipocytes in psWAT or dermal WAT of *Lmna*^{ADKO} mice following HFD feeding (Fig. 5C). In addition, we observed a striking loss of regulated and constitutive BMAT in HFD-fed *Lmna*^{ADKO} mice (Supplementary Fig. 5B–E), which was again correlated with higher cortical bone area fraction and thickness and increased trabecular thickness (Supplementary Fig. 5F–M). As predicted, the metabolic phenotype of *Lmna*^{ADKO} mice worsened with HFD feeding. Circulating glucose concentrations were elevated in fasted and random-fed states (Fig. 5D), whereas serum insulin concentrations were higher only in random-fed *Lmna*^{ADKO} mice (Fig. 5E). Adiponectin and leptin were essentially undetectable in *Lmna*^{ADKO} mice after 5 weeks of HFD feeding (Fig. 5F and G). Circulating triacylglycerol concentrations showed an upward trend (Fig. 5H), whereas serum glycerol concentrations were decreased (Fig. 5I), in female mice with adipocyte-specific *Lmna* deletion. Taken together, placing *Lmna*^{ADKO} mice on an HFD stimulates profound lipodystrophy, characterized by dysfunction in glucose and lipid homeostasis, which is highly reminiscent of lipodystrophy in humans with R482 mutations.

Adipose Tissue Develops in Young *Lmna*^{ADKO} Mice Postnatally and Is Progressively Lost With Aging

Patients with FPLD2 exhibit relatively normal adipose tissue development until puberty, at which point adipose tissue progressively deteriorates and/or is redistributed from the limbs to the head and neck (7,8,14). Thus, we next explored whether young mice with adipocyte-specific *Lmna* deletion develop adipose tissues postnatally. When observed at 4 weeks of age, psWAT and gWAT appeared normal upon gross examination (Fig. 6A and Supplementary Fig. 6A). Total body weight was unaffected by loss of lamin A/C in adipocytes at 4 weeks of age (Supplementary Fig. 6B). Although weight of psWAT mass was not different in either sex at 2 weeks of age, female *Lmna*^{ADKO} mice had reduced psWAT at 4 weeks of age, and both sexes had less psWAT at 6 weeks of age, compared with *Lmna*^{FL} controls (Fig. 6B). In histological examination of psWAT and gWAT, gross abnormalities were not detected (Fig. 6C), but histomorphometric analysis revealed smaller adipocytes in female but not male *Lmna*^{ADKO} mice at 4 weeks of age (Fig. 6D).

Livers of *Lmna*^{ADKO} mice at 4 weeks of age did not have an obvious difference in appearance (Fig. 6A and C and Supplementary Fig. 6A), and their weights were not statistically increased (Supplementary Fig. 6C). Whereas BAT appeared grossly similar between *Lmna*^{FL} and *Lmna*^{ADKO} mice at 4 weeks of age (Fig. 6A), histological analyses revealed an increase in lipid droplet size at that time (Fig. 6C). Weights of gWAT and spleen were not different between *Lmna*^{FL} and *Lmna*^{ADKO} mice at 4 weeks of age (Supplementary Fig. 6D and E). On the basis of our

observation of reduced circulating glycerol concentrations in adult *Lmna*^{ADKO} mice (Supplementary Fig. 2C), we measured responses to isoproterenol in *Lmna*^{FL} and *Lmna*^{ADKO} mice at 4 weeks of age. There were no differences in concentrations of circulating free glycerol at baseline between experimental groups, but *Lmna*^{ADKO} mice displayed a decreased lipolytic response to isoproterenol treatment at 60 min (Supplementary Fig. 6F).

We also observed an apparent increase in number of stromal cells in psWAT and gWAT of *Lmna*^{ADKO} mice at 4 weeks of age, which we hypothesized represented immune cell infiltration (Fig. 6C). However, FACS analysis of stromal vascular cells did not reveal differences in number of CD45⁺ or CD31⁺ cells between genotypes (Supplementary Fig. 6G and H). We also performed immunofluorescent staining to observe macrophages (Mac2) and adipocytes (Cav1) in psWAT tissue of *Lmna*^{FL} and *Lmna*^{ADKO} mice at 6 weeks of age but did not detect marked differences in number of Mac2⁺ cells between genotypes or in frequency of crown-like structures, a hallmark of adipocyte turnover (Fig. 6E). These data suggest that increased appearance of stromal vascular cells may be secondary to reduced size of adipocytes. We did, however, confirm our previous observation of smaller adipocytes in psWAT and gWAT depots of young *Lmna*^{ADKO} mice. Furthermore, *Lmna*^{ADKO} macrophages were larger and more clustered (Fig. 6E). Together these results demonstrate that adipose tissue develops postnatally in *Lmna*^{ADKO} mice and is progressively lost starting at ~4 weeks of age and continuing through sexual maturity, which closely mirrors FPLD2 disease progression in humans.

Lmna Deletion Does Not Affect Adipogenesis of Primary Mesenchymal Precursors

To interrogate molecular mechanisms underlying loss of adipose tissue in *Lmna*^{ADKO} mice, we induced deletion of *Lmna* in mesenchymal precursors isolated from *Lmna*^{FL} mice with an adenovirus expressing either Cre recombinase (Adeno-Cre) or GFP as a negative control (Adeno-GFP). PCR confirmed efficient recombination of the *Lmna* floxed allele with Adeno-Cre treatment (Supplementary Fig. 7A). *Lmna* deletion had no effect on adipogenesis or morphology of mature adipocytes even when cultured for up to 28 days (Fig. 7A), despite almost complete loss of lamin A/C protein (Fig. 7B).

Lamin A/C Deficiency Increases Lipolysis of Cultured Adipocytes

Next, we asked whether *Lmna* deletion in cultured adipocytes affects cellular function. We hypothesized that loss of lamin A/C in adipocytes might increase lipolysis based on the decrease in size of adipocytes in psWAT of *Lmna*^{ADKO} mice (Fig. 6D). Although lipolysis at baseline or after treatment with forskolin was not altered, we did observe a slight increase in glycerol secretion in *Lmna*-deficient adipocytes following stimulation with

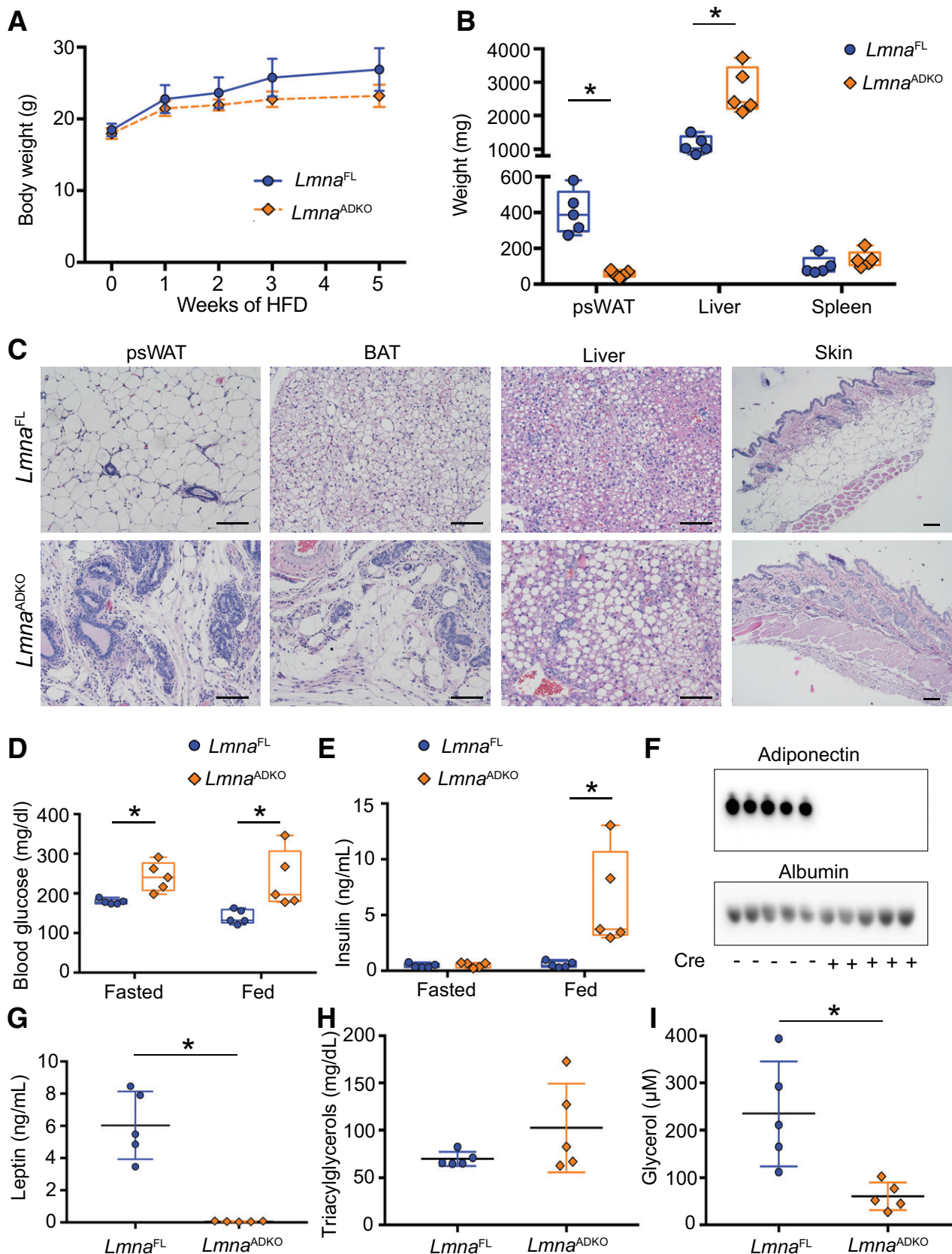


Figure 5—HFD challenge exacerbates the lipodystrophic phenotype of *Lmna*^{ADKO} mice. **A**: Body weights of female *Lmna*^{FL} and *Lmna*^{ADKO} mice over the course of 5 weeks of HFD feeding. **B**: Weights of psWAT, liver, and spleen in *Lmna*^{FL} and *Lmna*^{ADKO} mice after 5 weeks of HFD feeding. **C**: Representative histologic images of psWAT, BAT, liver, and skin of *Lmna*^{FL} and *Lmna*^{ADKO} mice stained with hematoxylin-eosin. Scale bars 100 μmol/L. **D** and **E**: Circulating glucose (**D**) and insulin concentrations (**E**) in HFD-fed *Lmna*^{FL} and *Lmna*^{ADKO} mice fed ad libitum or following an 8-h fast. **F**: Immunoblot of circulating adiponectin in serum of HFD-fed *Lmna*^{FL} and *Lmna*^{ADKO} mice. **G**–**I**: Circulating leptin (**G**), triacylglycerol (**H**), and glycerol (**I**) concentrations in serum of HFD-fed *Lmna*^{FL} and *Lmna*^{ADKO} mice. **P* < 0.05.

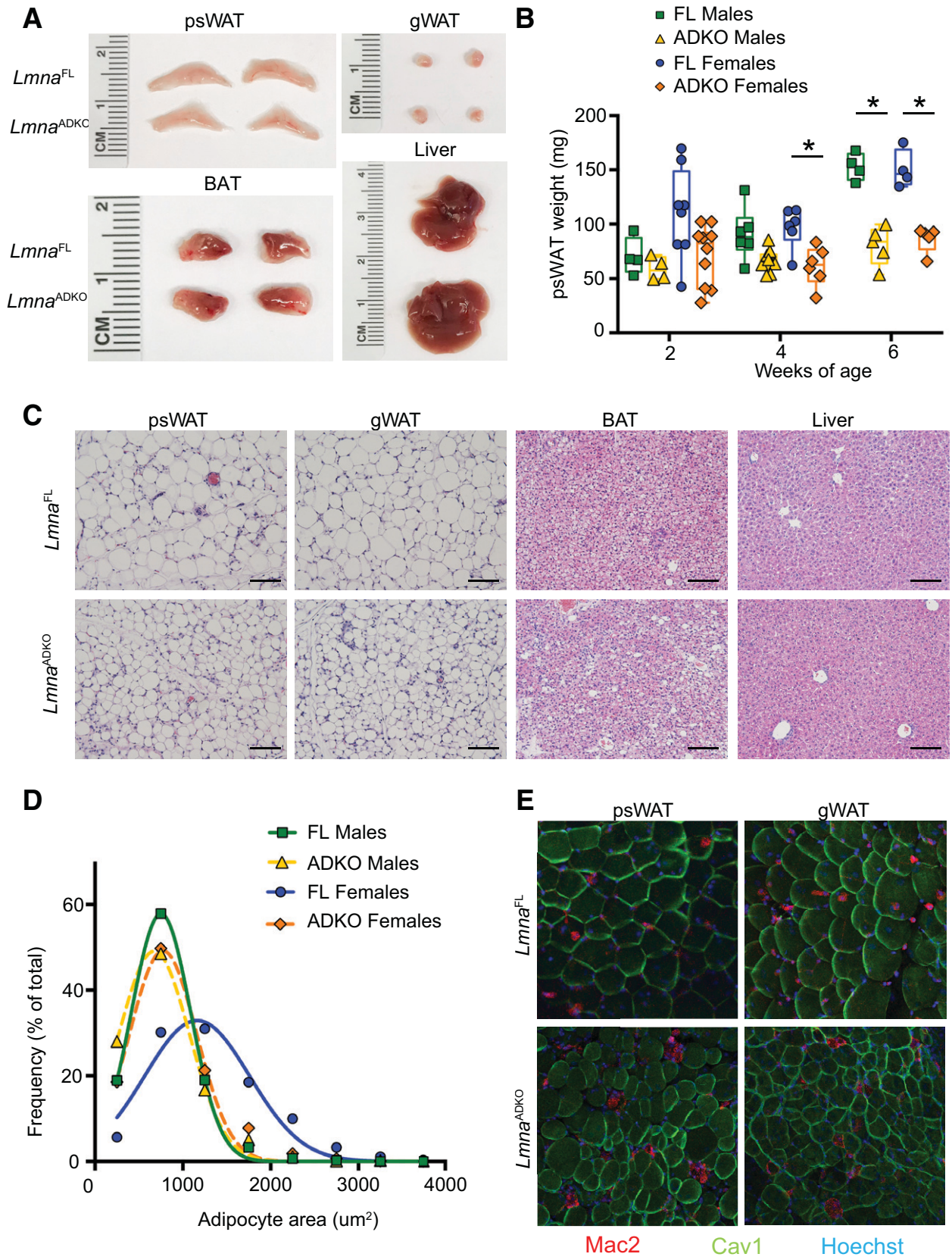


Figure 6—Adipose tissue develops postnatally in *Lmna*^{ADKO} mice and is progressively lost with aging. **A**: Representative images of indicated organs from female *Lmna*^{FL} and *Lmna*^{ADKO} mice 4 weeks of age. **B**: psWAT tissue weight at the indicated time points in *Lmna*^{FL} and *Lmna*^{ADKO} mice. **C**: Representative histologic images of the indicated organs stained with hematoxylin-eosin from female *Lmna*^{FL} and

isoproterenol or norepinephrine (Fig. 7C). Effects of lipolytic stimuli on glycerol release were correlated with corresponding increases in phosphorylated hormone-sensitive lipase, as well as perilipin and phosphorylation of protein kinase A substrates (Fig. 7D). Whereas total hormone-sensitive lipase was increased in adipocytes lacking lamin A/C, changes in ATGL or adiponectin were not observed (Fig. 7D). We then investigated fatty acid uptake in *Lmna*-deficient cultured adipocytes and found that functional lamin A/C is not required for entry into adipocytes of palmitic acid (Supplementary Fig. 7D). On the basis of our observation of increased circulating glucose and insulin concentrations in *Lmna*^{ADKO} mice (Fig. 5D and E), we considered whether *Lmna* deletion in cultured adipocytes would affect cellular responses to insulin stimulation; however, no differences were observed in baseline or insulin-stimulated glucose uptake or in stimulation of phosphorylated AKT (Supplementary Fig. 7B and C). These findings indicate that lamin A/C is not required for adipogenesis, but loss of lamin A/C does increase sensitivity of adipocytes to lipolytic stimuli.

DISCUSSION

Taken together, our findings demonstrate that adipocyte-specific loss of lamin A/C in mice yields a phenotype that closely mirrors that observed in human FPLD2 patients. In both cases, development of adipose tissues appears to occur normally, but depots are progressively lost during sexual maturation, with almost complete depletion at older ages. Lipoatrophy in *Lmna*^{ADKO} mice is accompanied by ectopic lipid accumulation in BAT and liver, as well as increased circulating glucose and insulin and decreased circulating concentrations of adiponectin, leptin, and glycerol. Furthermore, these mice demonstrate a striking metabolic inflexibility and appear unable to switch substrate oxidation between lipids and carbohydrates to meet their energetic needs. The metabolic dysfunction observed in *Lmna*^{ADKO} mice is not as extreme as that observed in FPLD2 patients or in other mouse models of lipoatrophy (34–38), even after 5 weeks of HFD; however, it is likely that a longer-term feeding of HFD would further worsen the impaired glucose and lipid homeostasis.

The major discrepancies between *Lmna*^{ADKO} mice and FPLD2 patients are the extent of lipodystrophy and effects on bone. Whereas *Lmna*^{ADKO} mice have increased cortical bone, we show herein that FPLD2 patients have widespread loss of skeletal bone mass and bone mineral density. We speculate that older *Lmna*^{ADKO} mice on a long-term HFD might have greater metabolic dysfunction

and a corresponding loss of cortical and trabecular bone. Alternatively, increased bone in *Lmna*^{ADKO} mice may be secondary to reductions in regulated and constitutive BMAT, another variable that differs between *Lmna*^{ADKO} mice and FPLD2 patients. A vast majority of FPLD2 cases are caused by a single point mutation (R482) in the *Lmna* gene, which is predominantly believed to act in a dominant-negative manner (40,41). Although *Lmna* haploinsufficiency does not cause either lipoatrophy or metabolic disease (26), the close parallels between *Lmna*^{ADKO} mice and FPLD2 patients suggest that the R482 mutation likely causes a loss of lamin A/C function.

Important questions that remain to be answered include the bases for progressive loss of WAT and BAT and whether sexual maturity plays a causative role, given the timing and sexual dimorphism. While it may be that postweaning development of adipocytes requires lamin A/C, and that adipose attrition simply reflects normal turnover without adipocyte replacement, our data provide strong support for a model in which lamin A/C is not necessary during adipogenesis for the embryonic/early postnatal development of adipose tissues. This idea is supported by our observation that lamin A/C is not required for adipogenesis of cultured primary mesenchymal precursors. We considered whether loss of lamin A/C might increase targeting of mature adipocytes by immune cells, but our evaluation of stromal vascular cell populations and tissue macrophages did not provide evidence to support this notion. Finally, it could be that lamin A/C deficiency is required for maintenance of the mature adipocyte phenotype and that apparent attrition is the result of negative energy balance or adipocyte death; however, our experiments suggest that mice lacking functional lamin do not have higher energy expenditure or altered food intake on a chow diet. Additional experiments will be required to distinguish between these possibilities, but the smaller adipocyte size observed in 4-week-old *Lmna*^{ADKO} mice and elevated lipolytic response to adrenergic stimuli of cultured adipocytes support a catabolic metabolic mechanism.

In summary, we report the novel finding that loss of lamin A/C in adipocytes causes a phenotype in mice similar to human FPLD2. Although the underlying genetics differ greatly between *Lmna*^{ADKO} mice and FPLD2, and opposing effects on bone and BMAT are observed, this is the first mouse model that mimics many of the characteristics of human FPLD2. *Lmna*^{ADKO} thus serves as a promising model to investigate molecular mechanisms that cause loss of progressive adipose tissue

Lmna^{ADKO} mice 4 weeks of age. Scale bars 100 μ mol/L. D: Histomorphometric quantification of adipocyte size in *Lmna*^{FL} and *Lmna*^{ADKO} mice 4 weeks of age. E: Confocal fluorescent micrographs of the indicated organs in *Lmna*^{FL} and *Lmna*^{ADKO} mice 6 weeks of age stained for macrophages (Mac2; red), adipocytes (Cav1; green), and cell nuclei (Hoechst; blue). **P* < 0.01.

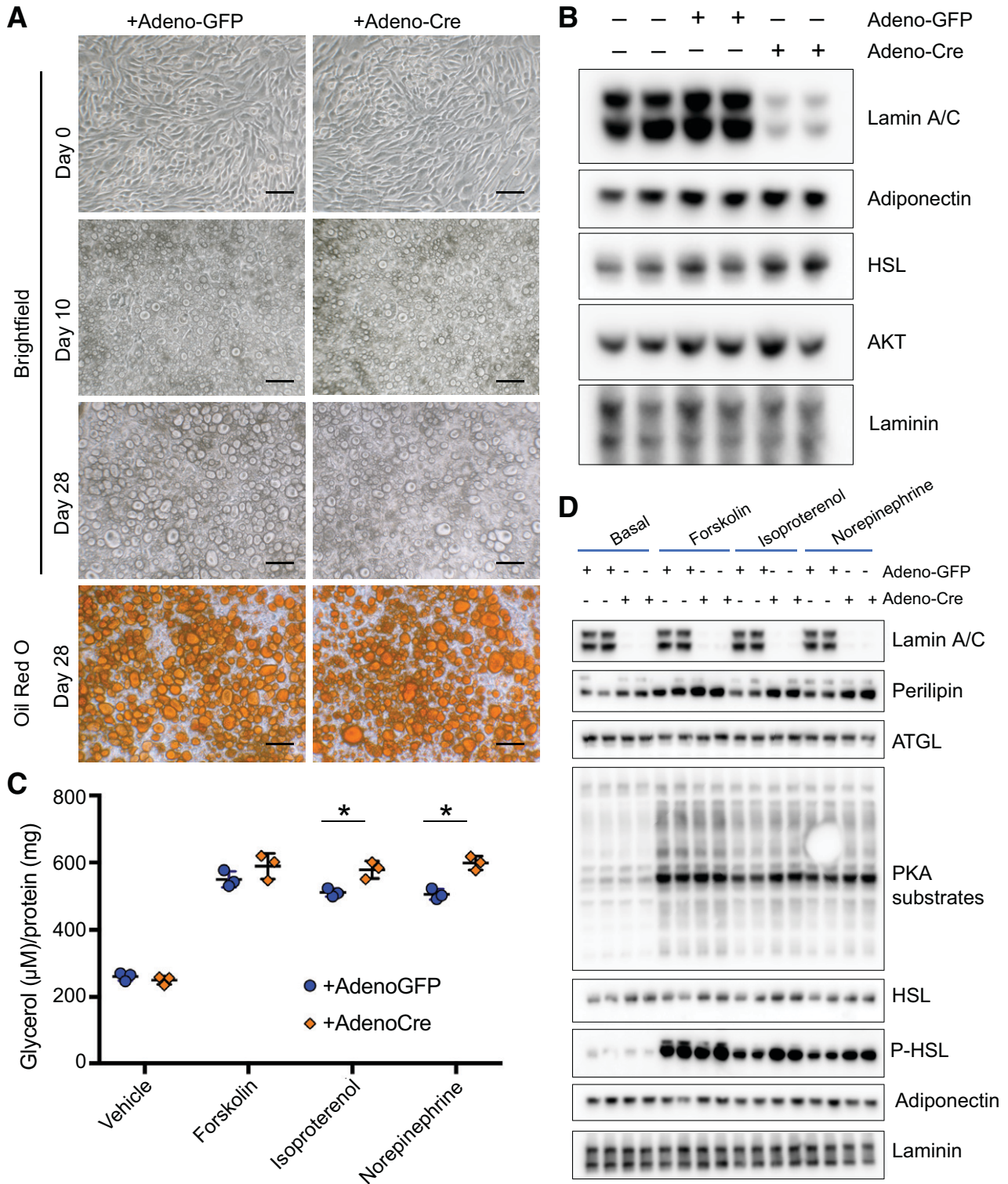


Figure 7—*Lmna* deletion does not affect adipogenesis of primary precursors. **A:** Primary *Lmna*^{FL} mesenchymal stem cells were treated with adeno-GFP or adeno-Cre prior to differentiation. Representative images at the indicated time points after induction of adipogenesis, with either brightfield microscopy or after staining neutral lipid with Oil Red O. Scale bars 50 µmol/L. **B:** Immunoblot of indicated proteins in mature adipocytes. **C:** Glycerol concentrations in conditioned media of mature adipocytes (*n* = 3) following treatment for 2 h with vehicle (DMSO), forskolin (5 µmol/L), isoproterenol (1 µmol/L), or norepinephrine (1 µmol/L). **D:** Immunoblot for the indicated proteins in mature adipocytes following 15-min treatment with vehicle (DMSO), forskolin (5 µmol/L), isoproterenol (1 µmol/L), or norepinephrine (1 µmol/L). **P* < 0.05. HSL, hormone-sensitive lipase; pHSL, phosphorylated hormone-sensitive lipase.

in FPLD2, as well as to develop new therapeutic strategies for lipodystrophy.

Acknowledgments. The authors thank members of the Oral and MacDougald laboratories for experimental advice and helpful discussions.

Funding. This work was supported by funds from the National Institutes of Health to D.P.B. (T32 HD007505 and T32 GM007863), K.T.L. (F32 DK122654), E.A.O. (R01 DK125513), and O.A.M. (R24 DK092759, R01 DK125513, and R01 DK121759), including grants from the National Institute of Diabetes and Digestive and Kidney Diseases to C.A.S.C. and R.L.S. (T32 DK101357), C.M.W. and K.T.L. (T32 DK071212), and R.L.S. (F32 DK123887). This work was also supported by postdoctoral fellowships from the American Diabetes Association to C.A.S.C. (1-18-PDF-064) and Z.L. (1-18-PDF-087) and from the Michigan Life Sciences Fellows program to C.M.W. This research was supported by the Michigan Mouse Metabolic Phenotyping Center (U2C DK110768), the Microscopy, Imaging, and Cellular Physiology Core (P30 DK020572), the Adipose Tissue Core of the Michigan Nutrition Obesity Research Center (P30 DK089503), and the University of Michigan Advanced Genomics Core. Histological analyses were supported by the National Institute of Arthritis and Musculoskeletal and Skin Diseases of the National Institutes of Health (P30 AR069620).

Duality of Interest. No potential conflicts of interest relevant to this article were reported.

Author Contributions. C.A.S.C., C.M.W., and O.A.M. conceived the experimental strategy, which was further developed by D.P.B., H.M., and E.A.O. and wrote the manuscript with input from all coauthors. D.P.B. conducted FACS, performed bone histology, and prepared bones for μ CT analysis. M.C.F.F. and A.E.R. conducted the human FPLD2 analyses. Z.L. analyzed the μ CT data. J.H. assisted with metabolic analyses. K.G. contributed to histologic analysis. R.L.S. contributed to animal studies. K.T.L. assisted with confocal microscopy. J.N.M. and R.D.A. performed immunoblot and quantitative polymerase chain reaction analyses. O.A.M. is the guarantor of this work and, as such, had full access to all the data in the study and takes responsibility for the integrity of the data and the accuracy of the data analysis.

References

1. Wojtanik KM, Edgemon K, Viswanadha S, et al. The role of LMNA in adipose: a novel mouse model of lipodystrophy based on the Dunnigan-type familial partial lipodystrophy mutation. *J Lipid Res* 2009;50:1068–1079
2. Boguslavsky RL, Stewart CL, Worman HJ. Nuclear lamin A inhibits adipocyte differentiation: implications for Dunnigan-type familial partial lipodystrophy. *Hum Mol Genet* 2006;15:653–663
3. Sullivan T, Escalante-Alcalde D, Bhatt H, et al. Loss of A-type lamin expression compromises nuclear envelope integrity leading to muscular dystrophy. *J Cell Biol* 1999;147:913–920
4. Kubben N, Voncken JW, Konings G, et al. Post-natal myogenic and adipogenic developmental: defects and metabolic impairment upon loss of A-type lamins. *Nucleus* 2011;2:195–207
5. Oldenburg AR, Delbarre E, Thiede B, Vigouroux C, Collas P. Dereglulation of Fragile X-related protein 1 by the lipodystrophic lamin A p.R482W mutation elicits a myogenic gene expression program in preadipocytes. *Hum Mol Genet* 2014;23:1151–1162
6. Akinci B, Meral R, Oral EA. Phenotypic and genetic characteristics of lipodystrophy: pathophysiology, metabolic abnormalities, and comorbidities. *Curr Diab Rep* 2018;18:143
7. Hussain I, Garg A. Lipodystrophy syndromes. *Endocrinol Metab Clin North Am* 2016;45:783–797
8. Garg A, Agarwal AK. Lipodystrophies: disorders of adipose tissue biology. *Biochim Biophys Acta* 2009;1791:507–513
9. Guillín-Amarelle C, Fernández-Pombo A, Sánchez-Iglesias S, Araújo-Vilar D. Lipodystrophic laminopathies: diagnostic clues. *Nucleus* 2018;9:249–260
10. Dunnigan MG, Cochrane MA, Kelly A, Scott JW. Familial lipodystrophic diabetes with dominant transmission. A new syndrome. *Q J Med* 1974;43:33–48
11. Cao H, Hegele RA. Nuclear lamin A/C R482Q mutation in canadian kindreds with Dunnigan-type familial partial lipodystrophy. *Hum Mol Genet* 2000;9:109–112
12. Shackleton S, Lloyd DJ, Jackson SN, et al. LMNA, encoding lamin A/C, is mutated in partial lipodystrophy. *Nat Genet* 2000;24:153–156
13. Peters JM, Barnes R, Bennett L, Gitomer WM, Bowcock AM, Garg A. Localization of the gene for familial partial lipodystrophy (Dunnigan variety) to chromosome 1q21-22. *Nat Genet* 1998;18:292–295
14. Araújo-Vilar D, Victoria B, González-Méndez B, et al. Histological and molecular features of lipomatous and nonlipomatous adipose tissue in familial partial lipodystrophy caused by LMNA mutations. *Clin Endocrinol (Oxf)* 2012;76:816–824
15. Resende ATP, Martins CS, Bueno AC, Moreira AC, Foss-Freitas MC, de Castro M. Phenotypic diversity and glucocorticoid sensitivity in patients with familial partial lipodystrophy type 2. *Clin Endocrinol (Oxf)* 2019;91:94–103
16. Kwapich M, Lacroix D, Espiard S, et al.; Diamenord-AEDNL Working Group. Cardiometabolic assessment of lamin A/C gene mutation carriers: a phenotype-genotype correlation. *Diabetes Metab* 2019;45:382–389
17. Friesen M, Cowan CA. FPLD2 LMNA mutation R482W dysregulates iPSC-derived adipocyte function and lipid metabolism. *Biochem Biophys Res Commun* 2018;495:254–260
18. Wang AS, Kozlov SV, Stewart CL, Horn HF. Tissue specific loss of A-type lamins in the gastrointestinal epithelium can enhance polyp size. *Differentiation* 2015;89:11–21
19. Eguchi J, Wang X, Yu S, et al. Transcriptional control of adipose lipid handling by IRF4. *Cell Metab* 2011;13:249–259
20. Koo E, Foss-Freitas MC, Meral R, et al. The metabolic equivalent BMI in patients with familial partial lipodystrophy (FPLD) compared with those with severe obesity. *Obesity* 2021;29(2):274–278
21. Rim J-S, Mynatt RL, Gawronska-Kozak B. Mesenchymal stem cells from the outer ear: a novel adult stem cell model system for the study of adipogenesis. *FASEB J* 2005;19:1205–1207
22. Mori H, Prestwich TC, Reid MA, et al. Secreted frizzled-related protein 5 suppresses adipocyte mitochondrial metabolism through WNT inhibition. *J Clin Invest* 2012;122:2405–2416
23. Erickson RL, Hemati N, Ross SE, MacDougald OA. p300 coactivates the adipogenic transcription factor CCAAT/enhancer-binding protein alpha. *J Biol Chem* 2001;276:16348–16355
24. Li Z, Hardij J, Evers SS, et al. G-CSF partially mediates effects of sleeve gastrectomy on the bone marrow niche. *J Clin Invest* 2019;129:2404–2416
25. Scheller EL, Doucette CR, Learman BS, et al. Region-specific variation in the properties of skeletal adipocytes reveals regulated and constitutive marrow adipose tissues. *Nat Commun* 2015;6:7808–7815
26. Cutler DA, Sullivan T, Marcus-Samuels B, Stewart CL, Reitman ML. Characterization of adiposity and metabolism in Lmna-deficient mice. *Biochem Biophys Res Commun* 2002;291:522–527
27. Girousse A, Virtue S, Hart D, et al. Surplus fat rapidly increases fat oxidation and insulin resistance in lipodystrophic mice. *Mol Metab* 2018;13:24–29
28. Cox AR, Chernis N, Kim KH, et al. Ube2i deletion in adipocytes causes lipodystrophy in mice. *Mol Metab* 2021;48:101221
29. Gilardi F, Winkler C, Quignodon L, et al. Systemic PPAR γ deletion in mice provokes lipodystrophy, organomegaly, severe type 2 diabetes and metabolic inflexibility. *Metabolism* 2019;95:8–20
30. Cortés VA, Curtis DE, Sukumaran S, et al. Molecular mechanisms of hepatic steatosis and insulin resistance in the AGPAT2-deficient mouse model of congenital generalized lipodystrophy. *Cell Metab* 2009;9:165–176

31. Scheller EL, Rosen CJ. What's the matter with MAT? Marrow adipose tissue, metabolism, and skeletal health. *Ann N Y Acad Sci* 2014;1311:14–30
32. Garg A, Peshock RM, Fleckenstein JL. Adipose tissue distribution pattern in patients with familial partial lipodystrophy (Dunnigan variety). *J Clin Endocrinol Metab* 1999;84:170–174
33. Veldhuis-Vlug AG, Rosen CJ. Clinical implications of bone marrow adiposity. *J Intern Med* 2018;283:121–139
34. Moitra J, Mason MM, Olive M, et al. Life without white fat: a transgenic mouse. *Genes Dev* 1998;12:3168–3181
35. Wang F, Mullican SE, DiSpirito JR, Peed LC, Lazar MA. Lipoatrophy and severe metabolic disturbance in mice with fat-specific deletion of PPAR γ . *Proc Natl Acad Sci USA* 2013;110:18656–18661
36. Shimomura I, Hammer RE, Ikemoto S, Brown MS, Goldstein JL. Leptin reverses insulin resistance and diabetes mellitus in mice with congenital lipodystrophy. *Nature* 1999;401:73–76
37. Pajvani UB, Trujillo ME, Combs TP, et al. Fat apoptosis through targeted activation of caspase 8: a new mouse model of inducible and reversible lipoatrophy. *Nat Med* 2005;11:797–803
38. Sakaguchi M, Fujisaka S, Cai W, et al. Adipocyte dynamics and reversible metabolic syndrome in mice with an inducible adipocyte-specific deletion of the insulin receptor. *Cell Metab* 2017;25:448–462
39. Winzell MS, Ahrén B. The high-fat diet-fed mouse: a model for studying mechanisms and treatment of impaired glucose tolerance and type 2 diabetes. *Diabetes* 2004;53(Suppl. 3):S215–S219
40. Hegele RA, Cao H, Anderson CM, Hramiak IM. Heterogeneity of nuclear lamin A mutations in Dunnigan-type familial partial lipodystrophy. *J Clin Endocrinol Metab* 2000;85:3431–3435
41. Elzeneini E, Wickström SA. Lipodystrophic laminopathy: lamin A mutation relaxes chromatin architecture to impair adipogenesis. *J Cell Biol* 2017;216:2607–2610